Chemical Engineering Journal 347 (2018) 953–962

Contents lists available at ScienceDirect

Chemical Engineering Journal

journal homepage: www.elsevier.com/locate/cej

Hierarchical MgFe-layered double hydroxide microsphere/graphene composite for simultaneous electrochemical determination of trace Pb(II) and Cd(II)

Yue Ma[a,b], Yongchuang Wang[a,b], Donghua Xie[a,b], Yue Gu[a,b], Xinle Zhu[c], Haimin Zhang[a], Guozhong Wang[a], Yunxia Zhang[a,*], Huijun Zhao[a,d]

[a] Key Laboratory of Materials Physics, Centre for Environmental and Energy Nanomaterials, Anhui Key Laboratory of Nanomaterials and Nanotechnology, CAS Centre for Excellence in Nanoscience, Institute of Solid State Physics, Chinese Academy of Sciences, Hefei 230031, China
[b] University of Science and Technology of China, Hefei 230026, PR China
[c] Safety Assessment Department, China Institute of Veterinary Drug Control, Beijing 100081, China
[d] Centre for Clean Environment and Energy, Griffith University, Gold Coast Campus, Queensland 4222, Australia

HIGHLIGHTS

- The hierarchical MgFe-LDH/graphene composite was synthesized.
- The individual and simultaneous detection of Cd(II) and Pb(II) were studied.
- Low detection limit, high sensitivity and broad linear range were realized.
- The proposed sensor was successfully applied for the determination of Cd(II) and Pb(II) in real samples.

GRAPHICAL ABSTRACT

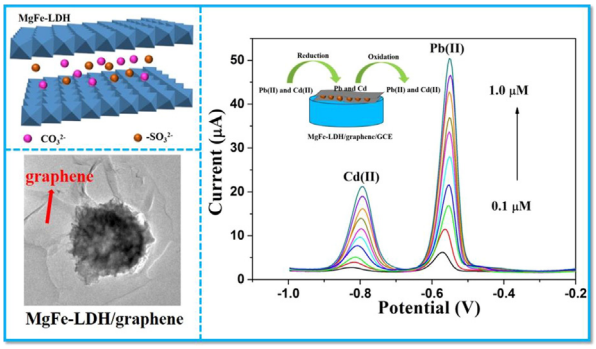

ARTICLE INFO

Keywords:
Hierarchical
MgFe-LDH/graphene
Cd(II)
Pb(II)
Simultaneous detection

ABSTRACT

Heavy metal contamination has been demonstrated to possess the severe threats toward the whole ecosystems and public security even at trace levels. Therefore, it is essential to exploit an ultrasensitive technique to determine the levels of heavy metal ions. In this work, hierarchical MgFe-layered double hydroxide (MgFe-LDH) microspheres have been successfully immobilized on the graphene nanosheets surface via a facile one-step hydrothermal route. Benefiting from the synergistic effects associated with high specific surface area, strong affinity of hierarchical MgFe-LDH architecture toward heavy metal ions, good electrical conductivity and effective electron transfer efficiency of graphene, the resulting composite (denoted as MgFe-LDH/graphene) is explored as an electrochemical sensor for simultaneous detection of Pb(II) and Cd(II) in aqueous medium. As a consequence, MgFe-LDH/graphene modified electrode exhibits low detection limit of 5.9 nM for Cd(II) and 2.7 nM for Pb(II), which are dramatically lower than the respective values of 3 ppb (27 nM) and 10 ppb (48 nM) in domestic water permitted by the World Health Organization (WHO). Meaningfully, the proposed electrochemical sensor shows specific recognition capability to Pb(II) and Cd(II), excellent reproducibility in repetitive measurements as well as feasibility in real water analysis.

* Corresponding author.
E-mail address: yxzhang@issp.ac.cn (Y. Zhang).

https://doi.org/10.1016/j.cej.2018.04.172
Received 27 February 2018; Received in revised form 20 April 2018; Accepted 24 April 2018
Available online 26 April 2018
1385-8947/

1. Introduction

With the rapid development of global industrial activities, heavy metal pollution has been evolved into a prominent environmental problem all over the world. Heavy metal ions, particularly Cd(II) and Pb (II), are alarming contaminants to environmental safety and public health due to their high toxicity even at low concentrations, non-biodegradability, and tendency of accumulation in the body via the food chain [1–9]. Hence, it is of vital importance to develop a feasible technique for detection of heavy metal ions from the viewpoint of environmental monitoring and human health concerns. With the increase of public awareness of environmental protection, diverse analytical techniques, such as atomic absorption spectroscopy [10,11], inductively coupled plasma optical emission spectroscopy [12–14], Raman spectrometry [15,16], spectrofluorimetry [17–20] and spectrophotometry [21] have been widely established for the detection of heavy metal ions in industrial wastewater and drinking water. In spite of high sensitivity and accuracy of these methods, they are not appropriate for on-site measurements on account of cumbersome and sophisticated apparatus, complicated pretreatment procedures and tedious analysis time. By contrast, electrochemical technique has received increasing attention in the analytical field due to its fascinating features such as simple handling, rapid response, low limit of detection (LOD), superior sensitivity and favorable selectivity [22–31].

Over the past decades, various materials such as inorganic, organic and bio-materials have been utilized to construct the electrochemical sensors for the determination of heavy metal ions. Nevertheless, most electrode materials suffer from some inherent limitations, e.g. low surface areas and poor electrical conductivity. Therefore, considerable efforts have been devoted to exploring advanced materials with well-defined structural design to improve the electrochemical sensing performances. As we all know, the sensitivity of electrochemical sensors is highly associated with the accumulating ability of modified electrode materials toward the target heavy metal ions. In this sense, layered double hydroxides (LDHs) are regarded as excellent candidates owing to flexible ion-exchangeability and tuneable compositions [32,33]. Particularly, surface hydroxyl groups and various interlayer anions of LDHs endow them with strong affinity to specific heavy metal ions, consequently contributing to enhanced electrochemical active sites [34–36]. Unfortunately, single LDHs usually possess rather poor electrical conductivity, which inhibits their potential applications in electrochemical sensing fields.

To overcome such limitation, one effective and feasible strategy has been proposed based on the rational integration of LDHs with conductive carbon materials. Among various carbon materials, graphene with a two-dimensional structure has been widely used in the environmental and energy fields on account of good electrical conductivity, large specific surface area, and excellent chemical/electrochemical stability [37–42]. On the one hand, ultrathin graphene nanosheets provide a platform for the rapid diffusion of electrolyte, facilitating the interfacial charge transfer during the electrochemical reaction. On the other hand, the incorporation of LDHs can effectively prevent the agglomeration of graphene and thereby is beneficial for full exposure of the electrode surface. Meanwhile, graphene is usually involved in abundant oxygen-containing functional groups, which are advantageous for preconcentrating heavy metal ions. Consequently, it is highly expected that hierarchical MgFe-LDH/graphene hybrid materials can greatly enhance the electrochemical detection toward heavy metal ions.

Based on the above considerations, in this work, a flower-like MgFe-LDH/graphene hierarchical architecture has been successfully prepared through a facile one-step hydrothermal route. The morphological and structural characteristics of the as-fabricated MgFe-LDH/graphene composite are systematically investigated through diverse characterization methods. The electrochemical sensing performances of the developed sensor, including sensitivity, LOD, linear range and selectivity, are investigated in detail by square wave anodic stripping voltammetry (SWASV). Furthermore, the repeatability and reproducibility study as well as real water sample analysis are also carried out to further evaluate the accuracy and reliability of the proposed sensor toward determination of Pb(II) and Cd(II).

2. Results and discussion

2.1. Morphological and structural characterization

The morphologies and structural details of the as-synthesized MgFe-LDH/graphene composite are investigated via field emission scanning electron microscope (FE-SEM) observation. As can be seen from Fig. 1a, the resulting composite displays a three-dimensional hierarchical structure, in which flower-like MgFe-LDH microspheres are composed of numerous ultrathin nanoflakes interlaced with each other. A closer observation reveals that MgFe-LDH microspheres are imbued with a layer of graphene voile. It should be mentioned that the crystallization

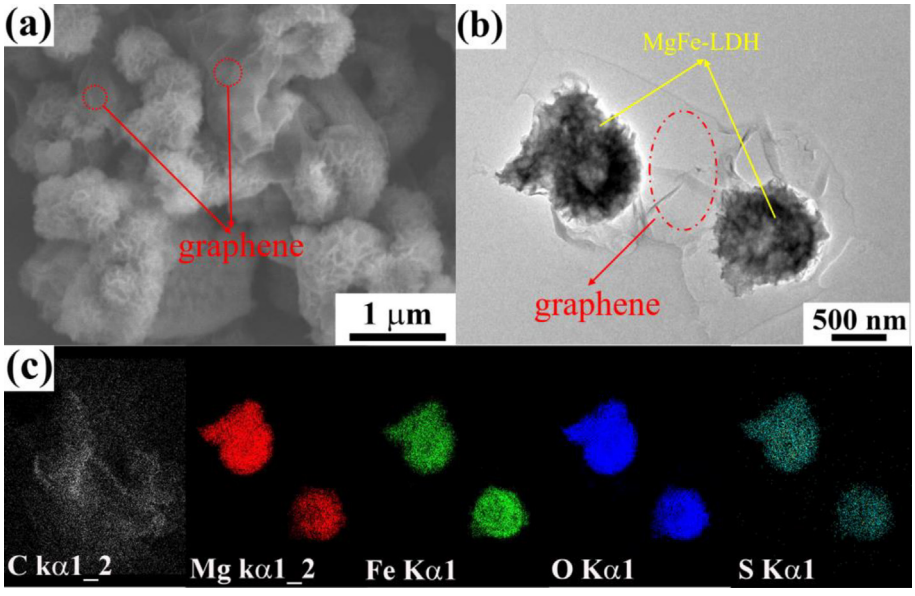

Fig. 1. (a) SEM image of MgFe-LDH/graphene composite; (b) and (c) TEM image of MgFe-LDH/graphene and the corresponding element mappings.

of MgFe-LDH and reduction of GO are fulfilled simultaneously during the hydrothermal process. The possible reason about the selective immobilization of MgFe-LDH microspheres onto the surface of graphene nanosheet can be attributed to plenty of the oxygen-containing groups with negative charge on GO surface, which can trap metal ions (namely Mg^{2+} and Fe^{3+}) through the electrostatic interaction and provide nucleation sites for the growth of MgFe-LDH, thereby forming the hierarchical MgFe-LDH/graphene hybrid materials. For comparison, FE-SEM morphologies of separate MgFe-LDH and graphene are also presented in Fig. S1. Similar to MgFe-LDH/graphene composite, bare MgFe-LDH consists of flower-like microspheres with diameters of several hundred nanometers; whereas graphene in the absence of MgFe-LDH displays plate-like morphology with lateral dimensions of several micrometers, accompanied by severe agglomeration. In addition, when $Mg(NO_3)_2{\cdot}6H_2O$ or $FeCl_3{\cdot}6H_2O$ is utilized as the single metal ion precursor, the resultant composites display irregular and unordered aggregation morphology, totally different from MgFe-LDH/graphene composite (Fig. S1c and d). The morphology of the as-synthesized MgFe-LDH/graphene composite is further investigated by transmission electron microscopy (TEM). From Fig. 1b, it is found that MgFe-LDH microspheres composed of numerous nanosheets are well dispersed on the surface of graphene, which effectively prevents individual graphene nanosheets from restacking and aggregating into larger particles, in good agreement with SEM observation. Although both MgFe-LDH and graphene are sheet-like structure, graphene looks more transparent while MgFe-LDH possesses dark contrast, which makes them easily differentiated in the resulting hybrid structure (pointed by the red and yellow arrows in Fig. 1b, respectively). Energy-dispersive X-ray spectroscopy (EDS) (Fig. S2) shows the coexistence of Mg, Fe, O, C and S elements in the resulting product, in which sulfur may be attributed to SDS residue in the LDH materials. In order to further corroborate the spatial distribution of every element inside MgFe-LDH/graphene composite, elemental mapping analyses are carried out. As shown in Fig. 1c, magnesium (red zone), iron (green zone), oxygen (blue zone) and sulfur (cyan zone) are homogeneously distributed throughout MgFe-LDH microspheres; while carbon (gray zone) derived from graphene spread all over the selected entire domain, suggesting the uniform anchoring of MgFe-LDH microspheres on graphene surface. Meanwhile, the exact atomic ratio of Mg to Fe is found to be about 3:1 based on inductively coupled plasma optical emission spectrometer (ICP-OES) analysis, which is well consistent with the feeding molar ratio of Mg/Fe precursors. To explore the textural properties of the as-synthesized MgFe-LDH/graphene composite, N_2 adsorption/desorption measurement is conducted. As displayed in Fig. S3, a type IV isotherm with H_3-type hysteresis loop is found, suggesting the existence of mesopores centered at ca. 3.7 nm. The corresponding pore volume and specific surface area are 0.11 $cm^3\,g^{-1}$ and 125 m^2/g, respectively. As comparison, the surface area of the obtained MgFe-LDH is also investigated and the corresponding specific surface area is determined to be 51 m^2/g, which is much smaller than that of MgFe-LDH/graphene composite. Hence, such a 3D hierarchical MgFe-LDH/graphene hybrid with high BET surface area and unique porous architecture may be anticipated to facilitate pre-enrichment for analytes, full exposure of electroactive surface to electrolyte, decrease of contact resistance between MgFe-LDH and graphene, consequently enhancing the resulting electrochemical performance [43].

Apart from the microstructural observation, the crystallographic phase and purity of the final composite are characterized by X-ray diffraction (XRD) patterns. As shown in Fig. 2a, for the pristine graphene (Curve I in Fig. 2a), the two peaks at around 26° and 44° can be attributed to the (002) and (101) reflections of hexagonal graphite carbon (JCPDS No.75-1621), respectively. As for MgFe-LDH/graphene, several new peaks appear at 11.3°, 23.1°, 34.2°, 38.9°, 46.4°, and 59.8°, corresponding to the diffractions from (003), (006), (012), (015), (018), and (110) planes of the $Mg_6Fe_2CO_3(OH)_{16}{\cdot}4H_2O$ phase, respectively (Curve II in Fig. 2a), confirming the coexistence of graphene and MgFe-LDH in the obtained composites. In addition, XRD patterns of the as-obtained products in the absence of $FeCl_3{\cdot}6H_2O$ or $Mg(NO_3)_2{\cdot}6H_2O$ are demonstrated in Fig. S4, confirming the successful fabrication of $Mg_5(CO_3)_4(OH)_2(H_2O)_4$/graphene and FeOOH/graphene composites. In order to distinguish the chemical bonding nature and functional groups of the resulting MgFe-LDH/graphene composite, Fourier transform infrared (FT-IR) measurement is performed and the corresponding spectrum is displayed in Fig. 2b. Obviously, a broad and intense absorption band appears at around 3420 cm^{-1}, originating from the stretching vibrations of hydroxyl groups. Meanwhile, the

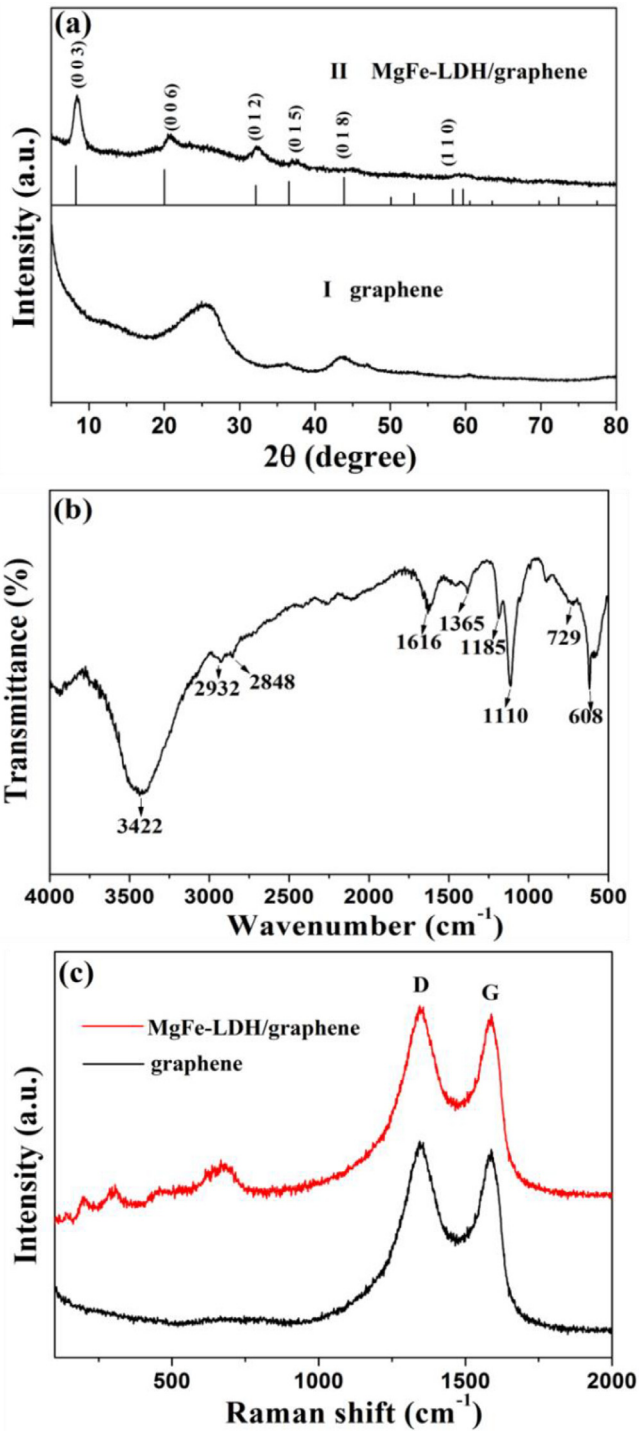

Fig. 2. (a) XRD patterns of graphene and MgFe-LDH/graphene; (b) FT-IR spectrum of MgFe-LDH/graphene; (c) Raman spectra of graphene and MgFe-LDH/graphene.

absorption peak at around 1616 cm^{-1} may be ascribed to hydroxyl deformation mode of absorbed water molecules. In addition to the characteristic bands related to hydroxyl groups, a sharp absorption peak at ca. 1365 cm^{-1} is also clearly observed, which is attributed to the asymmetric stretching mode of CO_3^{2-} [44,45]. Moreover, two bands in the lower wavenumber region (729 and 608 cm^{-1}) correspond to the stretching and bending vibrations of M–OH and M–O bonds (M = Mg and Fe) in the MgFe-LDH lattice. Furthermore, two bands at 1185 and 1110 cm^{-1} together with the other bands at 2932 and 2848 cm^{-1}, which originate from $–SO_3^{2-}$ group and the symmetric/antisymmetric stretching of $–CH_2$, respectively, indicate the residual of SDS in the as-prepared MgFe-LDH/graphene composite, consistent with EDS analysis [43,46]. Raman analysis is further utilized to provide the structural information about the resultant MgFe-LDH/graphene composite (Fig. 2c). For bare graphene, two characteristic bands at 1351 cm^{-1} (D-band) and 1589 cm^{-1} (G-band) are found. In the case of MgFe-LDH/graphene composite, several new Raman bands appear at ca. 197, 305 and 460 cm^{-1}, which can be assigned to the M-O-M linkage bonds, respectively; while the band at 670 cm^{-1} can be ascribed to intercalated CO_3^{2-}, revealing the successful incorporation of carbonate species into the interlayers of flower-like MgFe-LDH microsphere [47]. Considering the fact that the intensity ratio of D to G band (I_D/I_G) is associated with the disorder degree of carbon materials [2,39], in our case, I_D/I_G of MgFe-LDH/graphene approaches that of the pristine graphene (1.093 vs. 1.121). The finding suggests that the MgFe-LDH/graphene composite maintains the chemical/electrochemical stability of graphene, which is beneficial for electron transfer on the surface of electrode.

In an attempt to further investigate the chemical composition of the resulting product and valence states of different elements, X-ray photoelectron spectroscopy (XPS) technique are performed (Fig. 3). As shown in Fig. 3a, five peaks at 164.3, 284.9, 531.8, 711.2 and 1304.1 eV reveal the presence of S, C, O, Fe and Mg elements in the resultant composite. The high-resolution spectrum of C 1s (Fig. 3b) can be deconvoluted into four peaks located at 289.1 (C═O), 286.2 (C—O), 285.4 (C—OH) and 284.7 eV (C—C) [48]. Mg 1 s spectrum (Fig. 3c) displays an evident peak at 1304.3 eV [43]. Fe 2p (Fig. 3d) exhibits two obvious peaks at 711.1 and 724.7 eV, corresponding to Fe $2p_{3/2}$ and Fe $2p_{1/2}$, respectively. In addition, two satellite peaks at 718.7 and 733.6 eV indicate the existence of Fe(III) in the ultimate MgFe-LDH/graphene composite [49,50]. The results mentioned above confirm that the successful fabrication of MgFe-LDH/graphene composite.

2.2. Electrochemical characterization of different electrodes

The electrochemical behaviours of different electrodes are investigated by cyclic voltammetry (CV) in $[Fe(CN)_6]^{3-/4-}$ mixture containing 0.1 M KCl (Fig. 4a). In the case of graphene/GCE, the highest peak current (I_p) and the lowest potential separation (ΔE_P) are observed since graphene nanosheets can accelerate the diffusion of $[Fe(CN)_6]^{3-/4-}$ onto the surface of electrode. After modification with MgFe-LDH (i.e. MgFe-LDH/GCE), however, the peak current decreases greatly accompanied by increase of ΔE_P due to poor conductivity of MgFe-LDH. As for MgFe-LDH/graphene/GCE, the peak current exhibits a distinct enhancement compared with MgFe-LDH/GCE, indicating that graphene can afford effective electron transfer on the electrode surface. Moreover, the electrochemical behaviours of $Mg_5(CO_3)_4(OH)_2(H_2O)_4$/graphene/GCE and FeOOH/graphene/GCE are also investigated via a similar method. As shown in Fig. S5, the MgFe-LDH/graphene/GCE exhibits higher peak current compared with $Mg_5(CO_3)_4(OH)_2(H_2O)_4$/graphene/GCE and FeOOH/graphene/GCE. Electrochemical impedance spectroscopy (EIS) has been widely employed as a powerful method to explore the interface features of electrode [25,26]. Fig. 4b exhibits the typical Nyquist plots of four modified electrodes in $[Fe(CN)_6]^{3-/4-}$ mixture (1:1) containing 0.1 M KCl solution. Obviously, graphene/GCE possesses the smallest semicircle diameter at high frequency, suggesting the lowest charge transfer resistance (R_{ct}). In the case of MgFe-LDH/GCE, the semicircle diameter increases distinctly, indicating increased R_{ct} of MgFe-LDH. Interestingly, when MgFe-LDH is incorporated into graphene, the corresponding R_{ct} value decreases obviously compared to

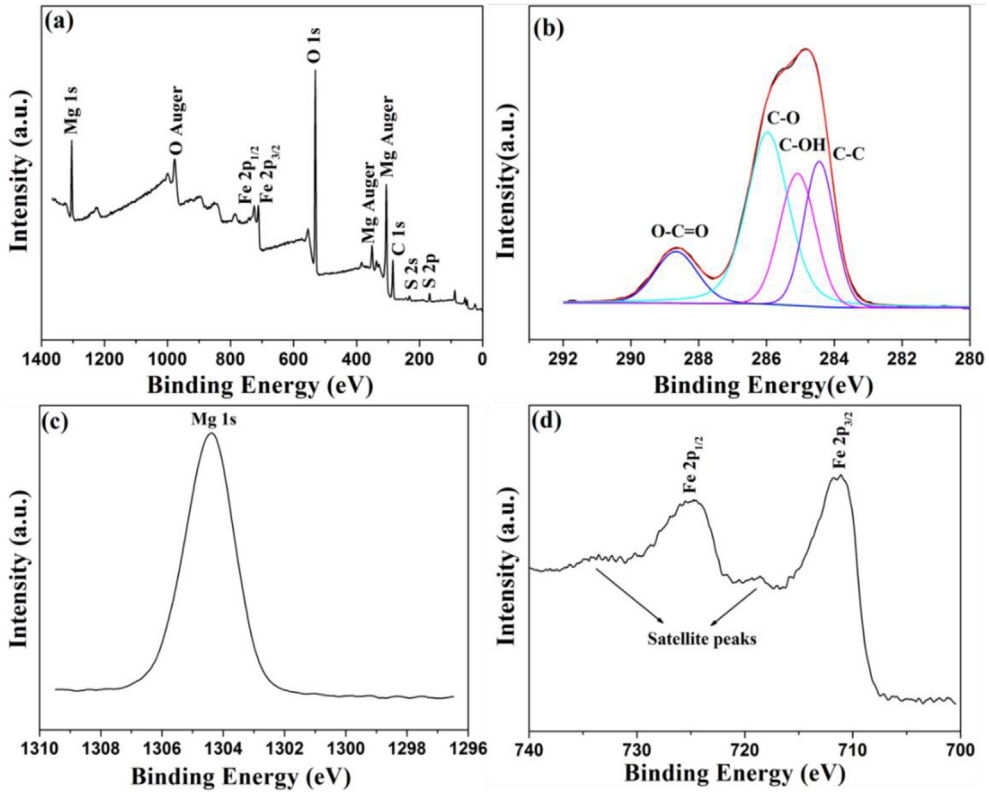

Fig. 3. XPS spectra of the as-fabricated MgFe-LDH/graphene composite: (a) survey spectrum; (b) C 1s; (c) Mg 1s; (d) Fe 2p.

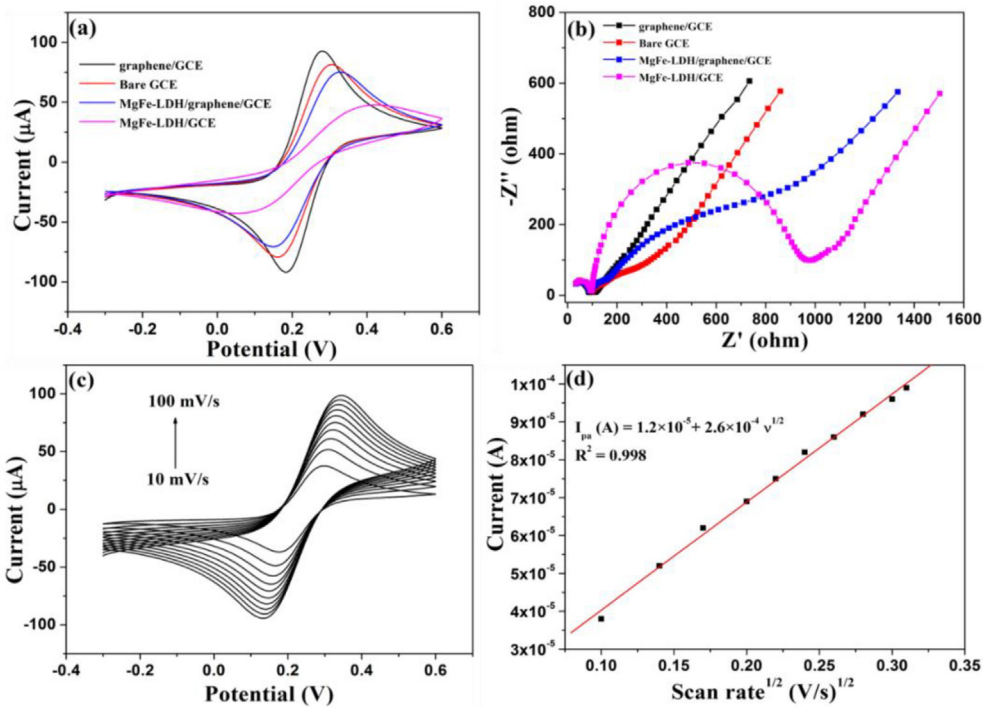

Fig. 4. (a) CVs and (b) EIS spectra of different electrodes in the solution containing 5.0 mM $[Fe(CN)_6]^{3-/4-}$ (1:1 M ratio) and 0.1 M KCl; (c) CVs of MgFe-LDH/graphene in the mixed solution containing 5.0 mM $[Fe(CN)_6]^{3-/4-}$ (1:1 M ratio) and 0.1 M KCl at different scan rates; (d) the linear relationship between the anodic peak currents and the square root of scan rate.

MgFe-LDH/GCE. These results clearly demonstrate that graphene can largely enhance the charge transfer efficiency of MgFe-LDH/graphene/GCE.

The real electrochemical active surface areas of NiFe-LDH NSAs/CC (Fig. 4c) are studied by cyclic voltammetry at various scan rates. Obviously, the anodic peak current (I_{pa}) linearly increases with increasing the square root of the scan rate (Fig. 4d). The liner equation can be determined as: I_{pa} (A) = $1.2 \times 10^{-5} + 2.6 \times 10^{-4}\ \nu^{1/2}$ ($R^2 = 0.998$). Therefore, the electrochemical surface areas can be calculated according to the Randles-Sevcik equation [51,52]:

$$I_{pa} = (2.69 \times 10^5) n^{3/2} A C D^{1/2} \nu^{1/2}$$

where I_{pa}, n, A, D, ν, and C represent the anodic oxidation peak current (A), electron-transfer number, effective surface area of the working electrode, diffusion coefficient of $K_3[Fe(CN)_6]$ in 0.1 M KCl (7.60×10^{-6} cm^2 s^{-1}), scan rate (V s^{-1}), concentration of the probe molecule (mol cm^{-3}), respectively. In contrast, the electrochemical active surface areas of bare GCE, graphene/GCE and MgFe-LDH/GCE electrodes are also investigated under the identical conditions (Fig. S6). As a consequence, the electrochemical active surface areas for graphene/GCE, bare GCE, MgFe-LDH/graphene/GCE, and MgFe-LDH/GCE electrodes are 0.11, 0.088, 0.071 and 0.042 cm^2, respectively. That is to say, the effective hybrid of MgFe-LDH and graphene may be conducive to provide an enhanced electrochemical behavior, reflected by high peak currents and smooth electron transfer process as well as large electrochemical active surface area.

2.3. Optimization of experimental conditions

To the best of our knowledge, SWASV is considered to be the most sensitive electroanalytic technique due to relatively low background noise. As we all know, the supporting electrolytes are of great importance to acquire the excellent sensing performance. Hence, the effect of different supporting electrolytes on SWASV response is studied to optimize the experimental conditions. Fig. 5a reveals the voltammetric behavior to two target metal ions at pH 6.0 in three different supporting electrolytes, i.e. 0.1 M NH_4Cl-HCl, phosphate buffer solution (PBS), and acetate buffer solution. It can be found that the largest peak current is obtained for two target metal ions in acetate buffer solution. Thus, 0.1 M acetate buffer solution is employed in the following experiments.

Taking into account the fact that pH value of the electrolyte solution exerts a significant influence on the accumulation of heavy metal ions on the electrode materials, the voltammetric responses of Pb(II) and Cd(II) (each of 1.0 μM) are investigated under varying pH. It can be found that the stripping currents of Pb(II) and Cd(II) increase with the increase of solution pH and then reach the maximum value at pH 6.0, followed by a minor decrease up to pH 7.0 (Fig. 5a). The specific pH-dependent behavior can be explained by the affinity variation between MgFe-LDH/graphene and heavy metal ions under various pH, consistent with the previous reports, in which the sorption capacities of Pb(II) and Cd(II) are stronger under near-neutral conditions [2,25,53]. Under low pH (4.0), poor current response may be correlated with the protonation of the functional groups on MgFe-LDH/graphene/GCE surface, weakening the adsorption of heavy metal ions; with increasing pH to 6.0, the increment in stripping peak currents can be attributed to favorable electrostatic attraction and surface complexation as a result of the deprotonation effect; whereas, under pH 7.0, the stripping currents for both Pb(II) and Cd(II) display a slight decrease, which may be correlated with the hydrolysis reaction of heavy metal ions, interfering with their accumulation on the surface of electrode. In view of the best current response, as a consequence, pH 6.0 is selected for the following experiments.

During stripping measurements, the appropriate deposition potential is of great concern to acquire the superior sensing performance. Accordingly, the influence of deposition potentials on the stripping currents is explored in 0.1 M acetate buffer solution at pH 6.0. As demonstrated in Fig. 5b, the stripping signals for both Pb(II) and Cd(II) increase with increasing potentials from −1.3 to −1.1 V, reach the apex at −1.1 V and then decrease gradually at more positive deposition potentials than −1.1 V. The phenomenon might be associated with the competitive generation of hydrogen gas at a more negative potential and the incomplete reduction of Pb(II) and Cd(II) on the MgFe-LDH/graphene/GCE surface at more positive deposition potentials [26]. Meanwhile, the deposition time is another critical parameter which affects the stripping peak current of MgFe-LDH/graphene/GCE. As depicted in Fig. 5c, the peak currents of Pb(II) and Cd(II) almost increase

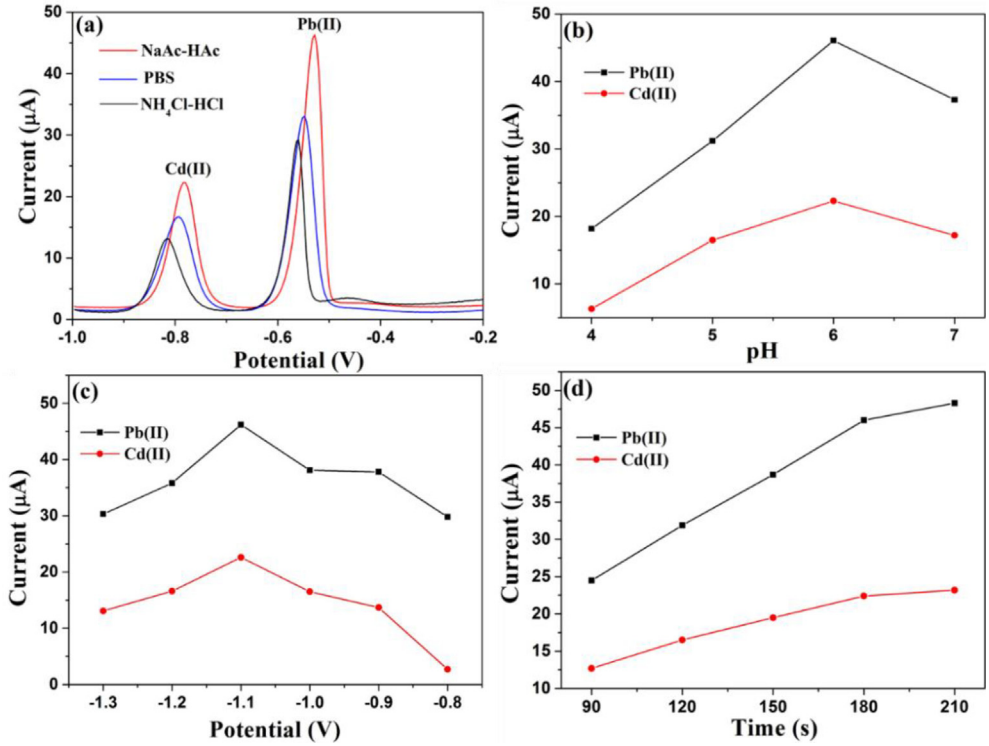

Fig. 5. Influence of various experimental parameters on SWASV response of MgFe-LDH/graphene/GCE toward Pb(II) (1 μM, black line) and Cd(II) (1 μM, red line): (a) supporting electrolytes; (b) pH; (c) deposition potential; (d) deposition time.

linearly with the deposition time from 90 to 180 s; while the two curves tend to be level off with prolonging deposition time up to 210 s, suggesting the approaching saturation of surface active sites due to the excessive accumulation of analytes on the MgFe-LDH/graphene/GCE surface. Based on the results mentioned above, −1.1 V and 180 s are employed as the optimal stripping potential and deposition time, respectively, in the following Pb(II) and Cd(II) sensing. In addition, other parameters including amplitude, frequency and step potential are fixed at 25 mV, 25 Hz and 4 mV, respectively.

2.4. Stripping response of lead and cadmium at various electrodes

The SWASV signals of Pb(II) and Cd(II) at diverse electrodes are examined under the above optimized operational conditions, in which the concentrations of two heavy metal ions are fixed at 1.0 μM. It should be noted that oxidation potentials of Pb and Cd are −0.55 and −0.8 V, respectively. From Fig. 6, bare GCE (black curve) displays the lowest peak currents. For MgFe-LDH (blue curve) and graphene (green curve) modified GCE, the stripping peak currents present an obvious enhancement compared to bare GCE, which can be correlated with high affinity of graphene and MgFe-LDH for the target heavy metal ions. In addition, $Mg_5(CO_3)_4(OH)_2(H_2O)_4$/graphene and FeOOH/graphene modified GCE exhibit smaller stripping peak currents as compared to MgFe-LDH/graphene modified GCE (Fig. S7). Specifically, among the investigated six electrodes, MgFe-LDH/graphene modified GCE (red curve) possesses the highest and sharpest stripping currents toward Pb (II) and Cd(II), revealing the synergistic amplification effect after the effective anchoring of MgFe-LDH on graphene surface. Consequently, the developed MgFe-LDH/graphene/GCE can be utilized as the promising electrochemical sensing probe for the detection of Pb(II) and Cd (II). The enhanced electrochemical response of the MgFe-LDH/graphene composite towards the target heavy ions might be derived from the following collective effects: (i) the specific 3D hierarchical characteristic ensures the maximum exposure of surface active sites, beneficial for the effective enrichment of Pb(II) and Cd(II); (ii) the abundant

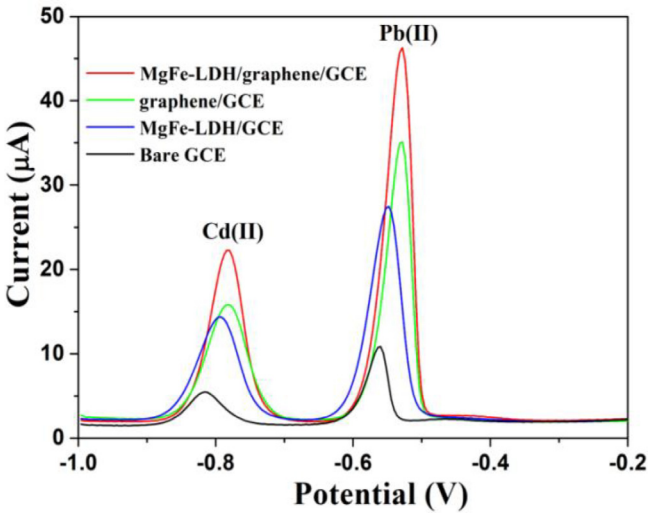

Fig. 6. SWASV curves of Cd(II) and Pb(II) (each of 1.0 μM) at different electrodes in 0.1 M acetate buffer solution (pH 6.0).

mesopores in the resulting MgFe-LDH/graphene architectures offer unobstructed mass diffusion channels for the electrolyte ions, contributing to their high electrochemical activity; (iii) abundant surface hydroxyl groups and various interlayer anions (e.g. CO_3^{2-} and $-SO_3^-$) inside MgFe-LDH provide more chance toward trapping of metal ions [34]; (iv) the in-situ anchoring of flower-like MgFe-LDH microspheres on conductive graphene surface reduces the contact resistance between MgFe-LDH and graphene, which can effectively overcome the weakness of MgFe-LDH in terms of relatively poor conductivity, ultimately guaranteeing highly efficient redox reactions.

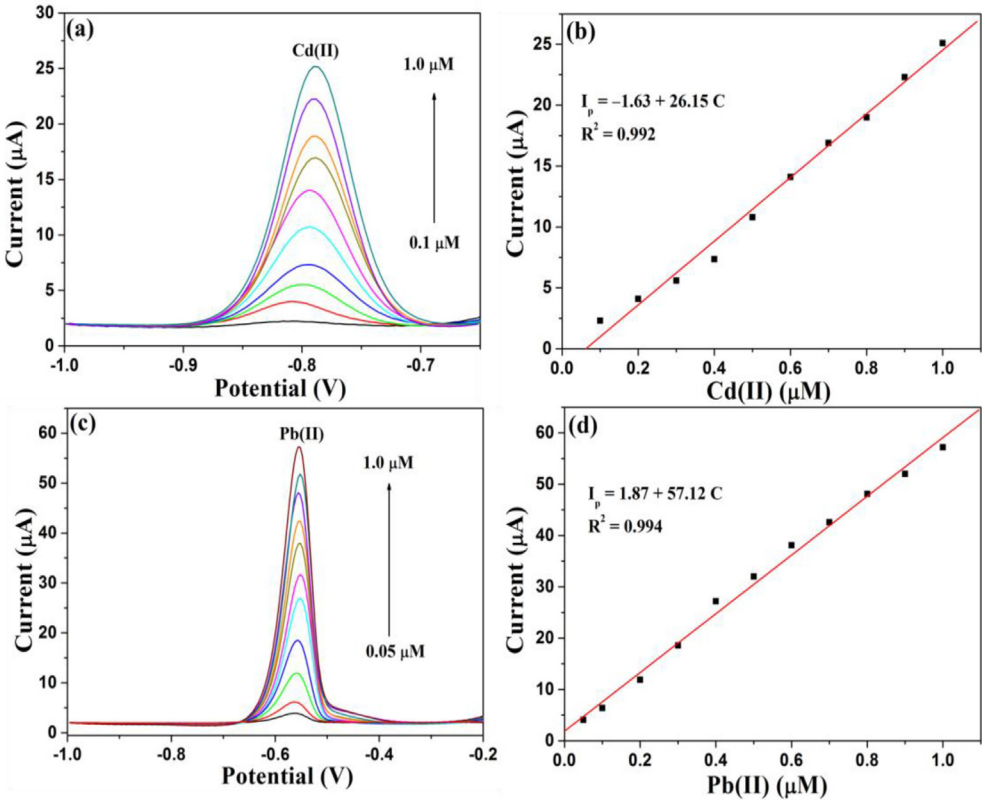

Fig. 7. SWASV responses of the MgFe-LDH/graphene/GCE for the individual analysis of (a) Cd(II) over a concentration range of 0.1 to 1.0 μM and (c) Pb(II) over a concentration range of 0.05 to 1.0 μM; the corresponding linear relationships between I_p and concentration of the target heavy metal: (b) Cd(II) and (d) Pb(II).

2.5. Electrochemical sensing behaviours of Pb(II) and Cd(II) at MgFe-LDH/graphene/GCE

In view of the favorable electroanalytical response, the developed MgFe-LDH/graphene modified GCE is attempted to the quantitative determination of Pb(II) and Cd(II) using SWASV under the optimal conditions. As shown in Fig. 7a, well-defined peaks at about −0.8 V are observed in the presence of the individual Cd(II) with various concentration, which corresponds to the oxidation potential of cadmium. Furthermore, the stripping currents are affinitive to Cd(II) concentration over a range of 0.1 to 1.0 μM (Fig. 7b). The linear equation is described as: $I_p = -1.63 + 26.15C$ ($R^2 = 0.992$). As a consequence, the sensitivity and LOD can be calculated to be 26.15 μA μM^{-1} and 4.7 nM (3σ method), respectively. Likewise, the SWASV response of the proposed MgFe-LDH/graphene/GCE toward Pb(II) is also explored using the similar method. As can be seen from Fig. 7c, Pb(II) is prominently identified at the potential of ca. −0.56 V with sharp peaks. Additionally, the stripping currents increase proportionally with the increasing concentration of Pb(II) ranging from 0.05 to 1.0 μM, in which the linear relationship can be evaluated as $I_p = 1.87 + 57.12C$ ($R^2 = 0.994$) (Fig. 7d). Accordingly, the corresponding sensitivity and LOD are calculated to be 57.12 μA μM^{-1} and 2.3 nM, respectively.

Besides the individual detection of Pb(II) or Cd(II), the resulting MgFe-LDH/graphene modified GCE are further successfully utilized to their simultaneous electrochemical analysis. Fig. 8 presents SWASV responses of Pb(II) and Cd(II) mixture under the optimal conditions. Apparently, two separate and well-resolved peaks are observed (Fig. 8a) at around −0.56 and −0.8 V for Pb(II) and Cd(II), respectively. It is noted that there is almost no shift about the stripping peak positions of coexisting Pb(II) and Cd(II) as compared to their individual determination, suggesting that mutual interference between Pb(II) and Cd(II) is very minimal. Since two peaks are completely separated, it is very likely for the proposed MgFe-LDH/graphene/GCE to identify simultaneously Pb(II) and Cd(II). As expected, the stripping peak currents of both Pb(II) and Cd(II) increase proportionally with increasing concentrations of Pb(II) and Cd(II). Meanwhile, good linear relationships are noticed for Pb(II) and Cd(II) ranging from 0.1 to 1.0 μM (Fig. 8b), which can be evaluated as $I_p = 2.05 + 49.86C$ and $I_p = -0.53 + 21.32C$ for Pb(II) and Cd(II), respectively. Consequently, LODs for Pb(II) and Cd(II) are calculated to be 2.7 nM and 5.9 nM, respectively, which are far below the respective threshold values of 3 ppb (27 nM) and 10 ppb (48 nM) in drinking water permitted by the WHO. It is therefore expected that the proposed electrochemical sensor can sufficiently meet the requirements of the practical environmental monitoring. Significantly, the analytical performance of the resulting MgFe-LDH/graphene composite in terms of LOD and linear range is comparable with and even better than other electrochemical sensors summarized in Table 1.

2.6. Interference study, repeatability, reproducibility, inter-day and intra-day performance

As well known, during the SWASV analysis, the interference ions may be also deposited onto the electrode surface together with the target metal ions, leading to an alteration of the stripping signals. Hence, the anti-interference capability of the proposed sensor is investigated by examining the stripping response variation in the presence of common metal ions. From Table S1, the relative stripping signal deviations for both Pb(II) and Cd(II) are less than < 3% in the absence or presence of Na(I), K(I), Mg(II), Ca(II), Al(III), Zn(II), Fe(II), Co(II) and Ni(II) at a concentration of 50-fold as much as that of Pb(II) and Cd(II), suggesting negligible influence from these coexisting ions. Such an excellent anti-interference ability might be correlated with high affinity of MgFe-LDH/graphene composite for Pb(II) and Cd(II) over other ions. However, the injection of 5-fold concentration of Cu(II) exerts severe influences on the stripping analysis of Pb(II) and Cd(II) (Fig. S8a), in which the stripping peak derived from Cd(II) almost

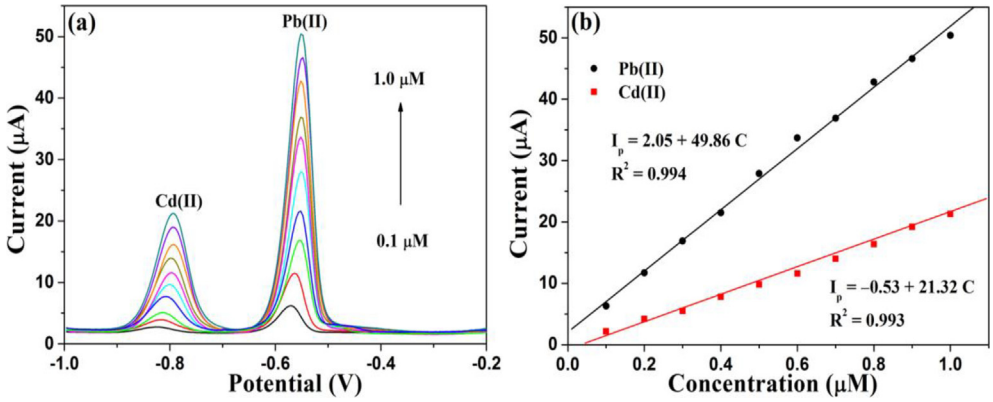

Fig. 8. SWASV response of MgFe-LDH/graphene/GCE for the simultaneous analysis of Cd(II) and Pb(II) over a concentration range of 0.1 to 1.0 μM; (b) the corresponding linear relationship between I_p and concentration of Cd(II) and Pb(II).

Table 1
Comparison of MgFe-LDH/graphene/GCE and other modified electrodes for the determination of Pb(II) and Cd(II).

Electrodes	Linear range (μM)		LOD (nM)		Refs.
	Cd(II)	Pb(II)	Cd(II)	Pb(II)	
BiNPs@NPCGS/GCE	0.08–0.8	0.06–0.6	4.1	3.2	[54]
$Pd_{1.5}$/PAC-900/GCE	0.5–5.5	0.5–8.9	41	50	[55]
Hg/FE/GCE	0.09–0.9	0.048–0.48	0.48	0.44	[56]
SNAC/GCE	0.09–4.8	0.09–5.7	24.4	5.7	[57]
NH_2-MCM-41/GCE	0.45–4.0	0.0024–1.2	8.9	0.97	[58]
Bi/NMC/GCE	0.018–0.89	0.0024–0.48	13.3	0.24	[59]
MgFe-LDH/graphene/GCE	0.1–1.0	0.1–1.0	5.9	2.7	This work

disappears; while the stripping current for Pb(II) reduces by about 77%. It should be mentioned that the stripping peak at −0.06 V derives from the oxidization potential of copper. Based on the previous reports, the significant interference induced by Cu(II) might be attributed to the generation of the Cu–Pb and Cu–Cd intermetallic compounds [25]. In the case of Hg(II), an obvious increase in stripping peak current of Pb (II) and Cd(II) are noticed even if equal concentration of Hg(II) is added (Fig. S8b). As reported previously, Hg(II) can be reduced during the deposition step, followed by the appearance of mercury film on the electrode surface, rendering Pb(II) and Cd(II) to be reduced more easily by forming an amalgam, which is ultimately responsible for the enhanced stripping currents of Pb(II) and Cd(II) [54].

To evaluate the repeatability of proposed sensor, a series of repetitive SWASV experiments (n = 15) are carried out in 0.1 M NaAc-HAc solution (pH 6.0) containing 0.5 μM Pb(II) and Cd(II) at same electrode. As shown in Fig. S9, there is no distinct alteration in the peak currents. And the relative standard deviations (RSDs) are calculated to be 2.97% for Cd(II) and 3.22% for Pb(II), respectively. In addition, the reproducibility of the fabricated MgFe-LDH/graphene/GCE is also studied at six different electrodes by checking the changes in the stripping currents of Pb(II) and Cd(II) (Fig. S10). As a result, RSDs of six parallel experiments are determined to be 3.78% for Pb(II) and 3.23% for Cd (II). The high repeatability and good reproducibility indicate that the developed MgFe-LDH/graphene modified electrode holds a great advantage in the future practical application. The inter-day (three repetitions of each concentration, three days) and intra-day (three repetitions of each concentration) performances are also investigated and the corresponding results are shown in Table S2. Both the intra-day and inter-day RSDs are lower than 5.0%, indicating that the developed sensor possesses acceptable precision.

2.7. Real sample analysis

The feasibility of the proposed sensing system is evaluated in practical environmental waters, including lake water (Dongpu Reservoir in Hefei City, China) and tap water. The collected water samples are treated via a filter membrane (0.22 μm) before experiments, followed by diluting with 0.1 M NaAc-HAc buffer solution (pH 6.0) at a volume ratio of 1:1. Subsequently, the samples are spiked with two various concentrations of Pb(II) and Cd(II) and then analyzed quantitatively by SWASV. Noticeably, each experiment is performed for five times and mean concentrations accompanied by RSDs are summarized in Table S3. As expected, the detected values of target metal ions are good consistent with the added concentrations and the routine ICP-OES measurements; meanwhile, the obtained RSD values (less than 4%) and average recoveries (ranging from 96.25 to 107.5%) are also acceptable. The high reliability and satisfactory recoveries endow the resulting MgFe-LDH/graphene modified electrode with the excellent feasibility toward Pb(II) and Cd(II) sensing in complex environment.

3. Conclusion

In summary, the hierarchical MgFe-LDH/graphene composite has been successfully fabricated through a facile hydrothermal method and further utilized to construct a novel electrochemical sensor for the simultaneous detection of trace Pb(II) and Cd(II) through SWASV. Electrochemical studies reveal that the developed MgFe-LDH/graphene composite exhibits enhanced electrochemical characteristics, including strong stripping peak and efficient charge transfer as well as large electrochemical active surface area as compared to the single-component counterparts. As expected, MgFe-LDH/graphene/GCE offers excellent electrochemical sensing performance toward simultaneous detection of trace Pb(II) and Cd(II) in terms of high sensitivity, broad linear range, low LOD, good selectivity, superior reproducibility and repeatability. The outstanding analytical property of the developed sensing system can be attributed to the integrated effects associated with specific 3D hierarchical architecture, high surface area, abundant mesoporous channels, good electrical conductivity of graphene, as well as strong affinity toward heavy metal ions. Furthermore, the proposed sensor can be applied to the determination of Pb(II) and Cd(II) in real water samples accompanied by satisfactory recoveries. All of these findings prefigure great prospect of MgFe-LDH/graphene-based electrochemical sensor in highly sensitive and reliable determination of Pb (II) and Cd(II).

Acknowledgements

This work was financially supported by The National Key R&D Program of China (2017YFA0207202), National Natural Science

Foundation of China (Grants 51572263, 51772299, 51472246) and Strategic Priority Research Program of the Chinese Academy of Sciences (Grant XDA09030200).

Appendix A. Supplementary data

Supplementary data associated with this article can be found, in the online version, at http://dx.doi.org/10.1016/j.cej.2018.04.172.

References

[1] L. Cui, J. Wu, H. Ju, Electrochemical sensing of heavy metal ions with inorganic, organic and bio-materials, Biosens. Bioelectron. 63 (2015) 276–286.
[2] J. Liu, X. Ge, X. Ye, G. Wang, H. Zhang, H. Zhou, Y. Zhang, H. Zhao, 3D graphene/δ-MnO_2 aerogels for highly efficient and reversible removal of heavy metal ions, J. Mater. Chem. A 4 (2016) 1970–1979.
[3] L. Kong, L. Yan, Z. Qu, N. Yan, L. Li, β-Cyclodextrin stabilized magnetic Fe_3S_4 nanoparticles for efficient removal of Pb(II), J. Mater. Chem. A 3 (2015) 15755–15763.
[4] K.Z. Elwakeel, A.A. El-Bindary, E.Y. Kouta, E. Guibal, Functionalization of polyacrylonitrile/Na-Y-zeolite composite with amidoxime groups for the sorption of Cu (II), Cd(II) and Pb(II) metal ions, Chem. Eng. J. 332 (2018) 727–736.
[5] S.B. Khan, M.M. Rahman, A.M. Asiri, H.M. Marwani, S.M. Bawaked, K.A. Alamry, Co_3O_4 co-doped TiO_2 nanoparticles as a selective marker of lead in aqueous solution, New J. Chem. 37 (2013) 2888–2893.
[6] S.B.K. Mohammed, M. Rahman, Hadi M. Marwani, Abdullah M. Asiri, Khalid A. Alamry, Malik Abdul Rub, Anish Khan, Aftab Aslam Parwaz Khan, Abdullah H. Qusti, Low dimensional Ni-ZnO nanoparticles as marker of toxic lead ions for environmental remediation, J. Ind. Eng. Chem. 20 (2014) 1071–1078.
[7] D. Yang, X. Liu, Y. Zhou, L. Luo, J. Zhang, A. Huang, Q. Mao, X. Chen, L. Tang, Aptamer-based biosensors for detection of lead(ii) ion: a review, Anal. Methods 9 (2017) 1976–1990.
[8] M.M.R. her Bahadar Khan, Hadi M. Marwani, Abdullah M. Asiri, Khalid A. Alamry, An assessment of zinc oxide nanosheets as a selective adsorbent for cadmium, Nanoscale Res. Lett. 8 (2013) 377–384.
[9] Z. Liu, F. Luo, X.J. Ju, R. Xie, Y.M. Sun, W. Wang, L.Y. Chu, Gating membranes for water treatment: detection and removal of trace Pb^{2+} ions based on molecular recognition and polymer phase transition, J. Mater. Chem. A 1 (2013) 9659–9671.
[10] D. Citak, M. Tuzen, A novel preconcentration procedure using cloud point extraction for determination of lead, cobalt and copper in water and food samples using flame atomic absorption spectrometry, Food Chem. Toxicol. 48 (2010) 1399–1404.
[11] E.L. Silva, P.d.S. Roldan, Simultaneous flow injection preconcentration of lead and cadmium using cloud point extraction and determination by atomic absorption spectrometry, J. Hazard. Mater. 161 (2009) 142–147.
[12] E.L. Silva, S. Roldan Pdos, M.F. Gine, Simultaneous preconcentration of copper, zinc, cadmium, and nickel in water samples by cloud point extraction using 4-(2-pyridylazo)-resorcinol and their determination by inductively coupled plasma optic emission spectrometry, J. Hazard. Mater. 171 (2009) 1133–1138.
[13] L. Zhao, S. Zhong, K. Fang, Z. Qian, J. Chen, Determination of cadmium(II), cobalt (II), nickel(II), lead(II), zinc(II), and copper(II) in water samples using dual-cloud point extraction and inductively coupled plasma emission spectrometry, J. Hazard. Mater. 239–240 (2012) 206–212.
[14] N.N. Meeravali, S.J. Jiang, A novel cloud point extraction approach using cationic surfactant for the separation and pre-concentration of chromium species in natural water prior to ICP-DRC-MS determination, Talanta 80 (2009) 173–178.
[15] J. Li, L. Chen, T. Lou, Y. Wang, Highly sensitive SERS detection of As^{3+} ions in aqueous media using glutathione functionalized silver nanoparticles, ACS Appl. Mater. Interfaces 3 (2011) 3936–3941.
[16] Y. Chen, Z.P. Chen, S.Y. Long, R.Q. Yu, Generalized ratiometric indicator based surface-enhanced raman spectroscopy for the detection of Cd^{2+} in environmental water samples, Anal. Chem. 86 (2014) 12236–12242.
[17] X. Fu, T. Lou, Z. Chen, M. Lin, W. Feng, L. Chen, "Turn-on" fluorescence detection of lead ions based on accelerated leaching of gold nanoparticles on the surface of graphene, ACS Appl. Mater. Interfaces 4 (2012) 1080–1086.
[18] T. Lai, E. Zheng, L. Chen, X. Wang, L. Kong, C. You, Y. Ruan, X. Weng, Hybrid carbon source for producing nitrogen-doped polymer nanodots: one-pot hydrothermal synthesis, fluorescence enhancement and highly selective detection of Fe (III), Nanoscale 5 (2013) 8015–8021.
[19] S. Shaily, A. Kumar, N. Ahmed, A coumarin–chalcone hybrid used as a selective and sensitive colorimetric and turn-on fluorometric sensor for Cd^{2+} detection, New J. Chem. 41 (2017) 14746–14753.
[20] H.N. Kim, W.X. Ren, J.S. Kim, J. Yoon, Fluorescent and colorimetric sensors for detection of lead, cadmium, and mercury ions, Chem. Soc. Rev. 41 (2012) 3210–3244.
[21] J. Zhu, Y.Q. Yu, J.J. Li, J.W. Zhao, Colorimetric detection of lead(ii) ions based on accelerating surface etching of gold nanorods to nanospheres: the effect of sodium thiosulfate, RSC Adv. 6 (2016) 25611–25619.
[22] W. Xiong, L. Zhou, S. Liu, Development of gold-doped carbon foams as a sensitive electrochemical sensor for simultaneous determination of Pb (II) and Cu (II), Chem. Eng. J. 284 (2016) 650–656.
[23] H. Dai, N. Wang, D. Wang, H. Ma, M. Lin, An electrochemical sensor based on phytic acid functionalized polypyrrole/graphene oxide nanocomposites for simultaneous determination of Cd(II) and Pb(II), Chem. Eng. J. 299 (2016) 150–155.
[24] S. Xiong, J. Xu, F. Xie, X. Hu, G. Gong, Z. Wu, L. Yao, Stripping analysis of Pb(II), Cd (II), Hg(II) and Cu(II) based on irradiated attapulgite/Ionic liquid composites, Chem. Eng. J. 316 (2017) 383–392.
[25] C. Gao, X.Y. Yu, R.X. Xu, J.H. Liu, X.J. Huang, AlOOH-reduced graphene oxide nanocomposites: one-pot hydrothermal synthesis and their enhanced electrochemical activity for heavy metal ions, ACS Appl. Mater. Interfaces 4 (2012) 4672–4682.
[26] L. Cui, J. Wu, H. Ju, Nitrogen-doped porous carbon derived from metal-organic gel for electrochemical analysis of heavy-metal ion, ACS Appl. Mater. Interfaces 6 (2014) 16210–16216.
[27] I. Ahmad, M.N. Arshad, M.M. Rahman, A.M. Asiri, T.A. Sheikh, F.M. Aqlan, Crystal structure of N′-[(E)-(2-hydroxynaphthalen-1-yl)methylidene] benzenesulfonohydrazide (HNMBSH) and its application as Pb^{2+} ion sensor by its fabrication onto glassy carbon electrode, Inorg. Chim. Acta 467 (2017) 297–306.
[28] M.N. Arshad, T.A. Sheikh, M.M. Rahman, A.M. Asiri, H.M. Marwani, M.R. Awual, Fabrication of cadmium ionic sensor based on (E)-4-Methyl- N ′-(1-(pyridin-2-yl) ethylidene)benzenesulfonohydrazide (MPEBSH) by electrochemical approach, J. Organomet. Chem. 827 (2017) 49–55.
[29] A. Khan, A.A.P. Khan, M.M. Rahman, A.M. Asiri, S.Y.M. Alfaifi, L.A. Taib, Toward facile preparation and design of mulberry-shaped poly(2-methylaniline)-$Ce_2(WO_4)_3$@CNT nanocomposite and its application for electrochemical Cd^{2+} Ion detection for environment remediation, Polym.-Plast Technol. Eng. 57 (2017) 335–345.
[30] A.A.P. Khan, A. Khan, M.M. Rahman, A.M. Asiri, M. Oves, Lead sensors development and antimicrobial activities based on graphene oxide/carbon nanotube/poly (O-toluidine) nanocomposite, Int. J. Biol. Macromol. 89 (2016) 198–205.
[31] G. Liu, J. Chen, X. Hou, W. Huang, A highly-sensitive electrochemical sensor for the simultaneous detection of Cd^{2+} and Pb^{2+} using liquid phase-exfoliated graphene, Anal. Methods 6 (2014) 5760–5765.
[32] C. Li, M. Wei, D.G. Evans, X. Duan, Layered double hydroxide-based nanomaterials as highly efficient catalysts and adsorbents, Small 10 (2014) 4469–4486.
[33] M. Shao, R. Zhang, Z. Li, M. Wei, D.G. Evans, X. Duan, Layered double hydroxides toward electrochemical energy storage and conversion: design, synthesis and applications, Chem. Commun. 51 (2015) 15880–15893.
[34] T.L.J.M. Gong, X.Q. Wang, X.L. Hu, L.Z. Zhang, Efficient removal of heavy metal ions from aqueous systems with the assembly of anisotropic layered double hydroxide nanocrystals@carbon nanosphere, Environ. Sci. Tenol. 45 (2011) 6181–6187.
[35] L. Ling, W.J. Liu, S. Zhang, H. Jiang, Achieving high-efficiency and ultrafast removal of Pb(II) by one-pot incorporation of a N-doped carbon hydrogel into FeMg layered double hydroxides, J. Mater. Chem. A 4 (2016) 10336–10344.
[36] J. Ali, H. Wang, J. Ifthikar, A. Khan, T. Wang, K. Zhan, A. Shahzad, Z. Chen, Z. Chen, Efficient, stable and selective adsorption of heavy metals by thio-functionalized layered double hydroxide in diverse types of water, Chem. Eng. J. 332 (2018) 387–397.
[37] D. Chen, H. Feng, J. Li, Graphene oxide: preparation, functionalization, and electrochemical applications, Chem. Rev. 112 (2012) 6027–6053.
[38] Y. Xu, G. Shi, X. Duan, Self-assembled three-dimensional graphene macrostructures: synthesis and applications in supercapacitors, Acc. Chem. Res. 48 (2015) 1666–1675.
[39] J. Xu, S. Gai, F. He, N. Niu, P. Gao, Y. Chen, P. Yang, A sandwich-type three-dimensional layered double hydroxide nanosheet array/graphene composite: fabrication and high supercapacitor performance, J. Mater. Chem. A 2 (2014) 1022–1031.
[40] J.L. Gunjakar, I.Y. Kim, J.M. Lee, N.S. Lee, S.J. Hwang, Self-assembly of layered double hydroxide 2D nanoplates with graphene nanosheets: an effective way to improve the photocatalytic activity of 2D nanostructured materials for visible light-induced O_2 generation, Energy Environ. Sci. 6 (2013) 1008.
[41] X. Long, J. Li, S. Xiao, K. Yan, Z. Wang, H. Chen, S. Yang, A strongly coupled graphene and FeNi double hydroxide hybrid as an excellent electrocatalyst for the oxygen evolution reaction, Angew. Chem. Int. Edit. 53 (2014) 7584–7588.
[42] R.M. Ma, W. Ma, C.Y. Wang, J.B. Liang, X.H. Liu, K.C. Zhou, T. Sasaki, A superlattice of alternately stacked Ni-Fe hydroxide nanosheets and graphene for efficient splitting of water, ACS Nano 9 (2015) 1977–1984.
[43] M. Shao, F. Ning, J. Zhao, M. Wei, D.G. Evans, X. Duan, Hierarchical layered double hydroxide microspheres with largely enhanced performance for ethanol electrooxidation, Adv. Funct. Mater. 23 (2013) 3513–3518.
[44] S. Ma, S.M. Islam, Y. Shim, Q. Gu, P. Wang, H. Li, G. Sun, X. Yang, M.G. Kanatzidis, Highly efficient iodine capture by layered double hydroxides intercalated with polysulfides, Chem. Mater. 26 (2014) 7114–7123.
[45] F. Mi, X. Chen, Y. Ma, S. Yin, F. Yuan, H. Zhang, Facile synthesis of hierarchical core-shell Fe_3O_4@MgAl-LDH@Au as magnetically recyclable catalysts for catalytic oxidation of alcohols, Chem. Commun. 47 (2011) 12804–12806.
[46] N.J. Kang, D.Y. Wang, A green functional nanohybrid: preparation, characterization and properties of a β-cyclodextrin based functional layered double hydroxide, J. Mater. Chem. A 1 (2013) 11376.
[47] C. Tang, H.S. Wang, H.F. Wang, Q. Zhang, G.L. Tian, J.Q. Nie, F. Wei, Spatially confined hybridization of nanometer-sized NiFe hydroxides into nitrogen-doped graphene frameworks leading to superior oxygen evolution reactivity, Adv. Mater. (2015).
[48] Y. Hou, M.R. Lohe, J. Zhang, S. Liu, X. Zhuang, X. Feng, Vertically oriented cobalt selenide/NiFe layered-double-hydroxide nanosheets supported on exfoliated graphene foil: an efficient 3D electrode for overall water splitting, Energy Environ. Sci. 9 (2016) 478–483.

[49] M. Gong, Y. Li, H. Wang, Y. Liang, J.Z. Wu, J. Zhou, J. Wang, T. Regier, F. Wei, H. Dai, An advanced Ni-Fe layered double hydroxide electrocatalyst for water oxidation, J. Am. Chem. Soc. 135 (2013) 8452–8455.
[50] L. Yu, H. Zhou, J. Sun, F. Qin, F. Yu, J. Bao, Y. Yu, S. Chen, Z. Ren, Cu nanowires shelled with NiFe layered double hydroxide nanosheets as bifunctional electrocatalysts for overall water splitting, Energy Environ. Sci. 10 (2017) 1820–1827.
[51] J. Yang, S. Gunasekaran, Electrochemically reduced graphene oxide sheets for use in high performance supercapacitors, Carbon 51 (2013) 36–44.
[52] T.A. Silva, H. Zanin, E. Saito, R.A. Medeiros, F.C. Vicentini, E.J. Corat, O. Fatibello-Filho, Electrochemical behaviour of vertically aligned carbon nanotubes and graphene oxide nanocomposite as electrode material, Electrochim. Acta 119 (2014) 114–119.
[53] M.R. Awual, M. Khraisheh, N.H. Alharthi, M. Luqman, A. Islam, M. Rezaul Karim, M.M. Rahman, M.A. Khaleque, Efficient detection and adsorption of cadmium(II) ions using innovative nano-composite materials, Chem. Eng. J. 343 (2018) 118–127.
[54] L. Cui, J. Wu, H. Ju, Synthesis of bismuth-nanoparticle-enriched nanoporous carbon on graphene for efficient electrochemical enalysis of heavy-metal ions, Chem. Eur. J. 21 (2015) 11525–11530.
[55] P. Veerakumar, V. Veeramani, S.M. Chen, R. Madhu, S.B. Liu, Palladium nanoparticle incorporated porous activated carbon: electrochemical detection of toxic metal ions, ACS Appl. Mater. Interfaces 8 (2016) 1319–1326.
[56] E. Nagles, V. Arancibia, C. Rojas, R. Segura, Nafion-mercury coated film electrode for the adsorptive stripping voltammetric determination of lead and cadmium in the presence of pyrogallol red, Talanta 99 (2012) 119–124.
[57] R. Madhu, K.V. Sankar, S.M. Chen, R.K. Selvan, Eco-friendly synthesis of activated carbon from dead mango leaves for the ultrahigh sensitive detection of toxic heavy metal ions and energy storage applications, RSC Adv. 4 (2014) 1225–1233.
[58] X. Dai, F. Qiu, X. Zhou, Y. Long, W. Li, Y. Tu, Amino-functionalized MCM-41 for the simultaneous electrochemical determination of trace lead and cadmium, Electrochim. Acta 144 (2014) 161–167.
[59] L. Xiao, H. Xu, S. Zhou, T. Song, H. Wang, S. Li, W. Gan, Q. Yuan, Simultaneous detection of Cd(II) and Pb(II) by differential pulse anodic stripping voltammetry at a nitrogen-doped microporous carbon/Nafion/bismuth-film electrode, Electrochim. Acta 143 (2014) 143–151.